LANGMUIR Article
Cite This: Langmuir 2018, 34, 8581−8590
pubs.acs.org/Langmuir

Solvent Effects on Tuning Pore Structures in Polyimide Aerogels

Nicholas Teo and Sadhan C. Jana*

Department of Polymer Engineering, The University of Akron, 250 South Forge Street, Akron, Ohio 44325-0301, United States

Supporting Information

ABSTRACT: This work evaluates the effects of solvents and a block copolymer surfactant on pore structures in polyimide aerogels synthesized via sol−gel reaction process. Specifically, cross-linked polyimide gel networks are synthesized in single or mixed solvents from a combination of dimethylformamide, *N*-methylpyrrolidone, and dimethylacetamide and supercritically dried to obtain aerogels. The bulk density, pore size, and mechanical properties of aerogels are determined. The results show that gel times are strongly dependent on the electron acceptance ability of the solvent system and concentration of the surfactant. At longer gel times, the polyimide strands coarsen and the pores in aerogel shift from predominantly mesoporous to macroporous state with corresponding reduction in compressive modulus. The block copolymer surfactant also slows down gelation and coarsens the polyimide strands but only weakly affects the compressive modulus of the aerogels.

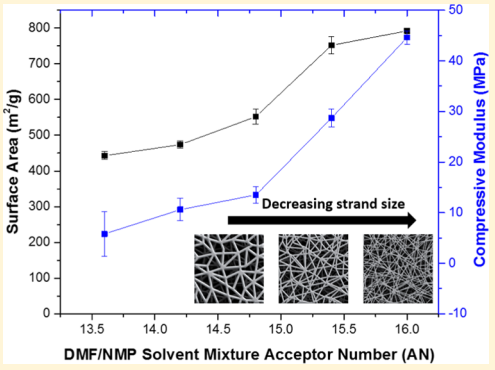

INTRODUCTION

Aerogels are known for their high porosity and high specific surface area. They have traditionally been used for thermal insulation,[1,2] although recent reports established their potential in airborne nanoparticle filtration.[3−7] Polymeric aerogels can be fabricated from physical gelation processes such as thermoreversible gelation, as in the case of syndiotactic polystyrene[8] or from the chemical sol−gel processes, such as in cases of silica,[9] polyurea,[10] and polyimide.[11] The choice of solvents in sol−gel processes indeed influences the morphology of resultant aerogels.[12,13] Rao et al.[14] reported that the choice of synthesis solvent affected the density, refractive index, surface area, pore volume, and porosity of silica aerogels. Leventis et al.[15] observed various microstructures in polyurea aerogels, e.g., string of beads in *N*,*N*-dimethylformamide, particle clusters in dimethylsulfoxide and fibrillar morphology in acetone. Gu et al.[13] reported strong dependence of polybenzoxazine aerogel building blocks, e.g., strands and spherical aggregates and corresponding specific surface area on choice of solvents and the reaction temperature.

A solvent affects the kinetics and equilibrium of chemical reactions. For example, S_N2 reactions can proceed at up to a 10^9 higher rate in dipolar aprotic solvents in comparison to that in protic solvents with similar macroscopic properties due to weaker anion solvating power and weaker structural effects of the aprotic solvents.[16,17] It is important to recognize that the macroscopic solvent properties, such as surface tension, permittivity, dielectric constants, solvent polarity, or refractive index, do not exert influence on molecular-level chemical reactivity.[18] The above macroscopic properties do not take into account solute−solvent interactions and their effects on the solvation and stabilization of the individual reactants, transition states, and the products in their polar environment.[19] Solvents form solvation shells around the solute molecules, which in turn lead to molecularly induced local inhomogeneities in the solvent environment, thus rendering dielectric or electrostatic approaches inadequate.[20] Empirical, semiquantitative measures were developed in an attempt to explain the solvent effects on reaction rates, such as in terms of Lewis basicity/acidity, nucleophilic/electrophilic nature, or electron donating/accepting capability. A number of empirical scales are used to rank the solvents. For example, Gutmann[21] proposed the donor number (DN) scale, measured on the basis of the negative enthalpy values of the 1:1 adduct formation between $SbCl_5$ in 1,2-dichloroethane to determine a solvent's nucleophilic, electron donating, or cation solvation tendency. Conversely, the acceptor number (AN) determines the electron accepting ability of the solvent, which was derived from the ^{31}P NMR measurement of triethylphosphine oxide dissolved in the desired solvent.[22] Both DN and AN have been shown to correlate well with other empirical scales, such as Kamlet and Taft's β-scale for nucleophilic ability (analogous to DN), Dimroth and Reichardt's $E_T(30)$, and Kosower's Z value[23] for electrophilic ability (analogous to AN).[24−26]

Traditionally, polyimides are synthesized using the Dupont two-step process.[27] The first step, the rate determining step, involves the reactions of a dianhydride with a diamine. In this step, nucleophilic acyl substitution reactions occur where the nitrogen in the amine group attacks the carbon of the carbonyl group,[28] thus forming a slightly negative activated complex that proceeds to form the polyamic acid. The polyamic acid group autocatalyzes the above reactions until an equilibrium is

Received: May 9, 2018
Revised: June 28, 2018
Published: June 29, 2018

DOI: 10.1021/acs.langmuir.8b01513
Langmuir 2018, 34, 8581−8590

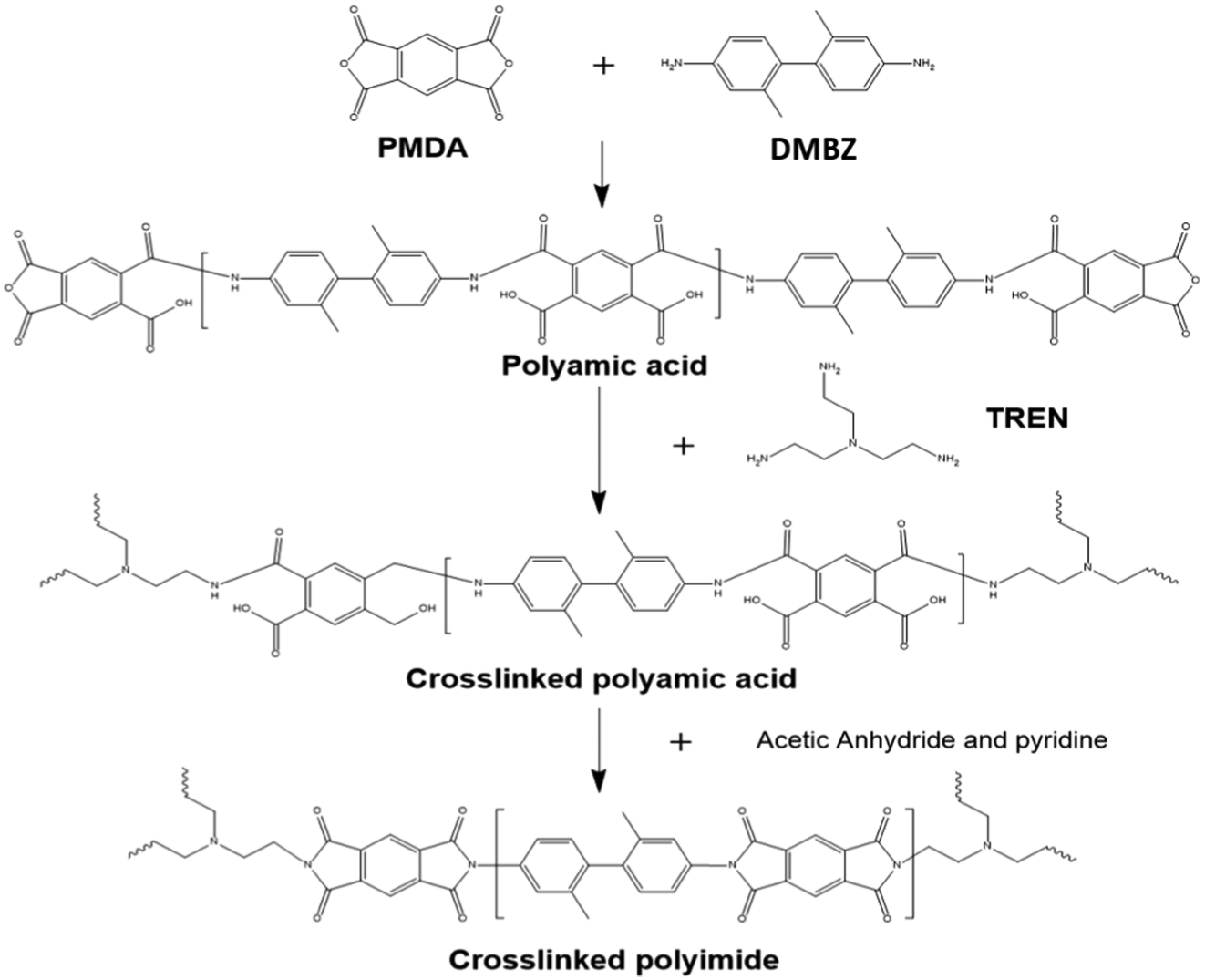

Figure 1. Reaction scheme for synthesis of polyimide cross-linked networks.

reached. The second step involves the chemical imidization of the polyamic acid with acetic anhydride as the dehydrating agent and pyridine as the catalyst.[29] These reactions are typically carried out in dipolar aprotic solvents as the anions are less solvated in these solvents compared with protic solvents, thus allowing for greater effectiveness in nucleophilic attack.[30]

In addition to diamines and dianhydrides, a trifunctional amine is used as a cross-linker to form a three-dimensional network structure that eventually produces polyimide gels. The molecular weight of the polymer chain increases until it is no longer soluble in the solvent. The reaction system undergoes polymerization-induced phase separation as the binodal and spinodal curves approach the experimental temperature with increasing molecular weight. The phase separation progresses until the system turns into a gel.

In this study, we investigated the effects of solvents and a block copolymer surfactant on polyimide aerogel morphology, bearing in mind that the solvents influence both the chemical kinetics of the polyimide reaction scheme and the thermodynamics of phase transition. The aim was to use the solvent environment to control and tune the pore size distribution in the aerogels. To our knowledge, the effect of surfactants on polyimide gelation has not been studied before. Such information will be useful in tuning of air permeability and airborne nanoparticle filtration efficiency of the final aerogels.[3−7] Recently, Teo and Jana[31] reported open-cell aerogel foams of syndiotactic polystyrene via emulsion-templating method, whereby surfactants were used to stabilize water-in-oil emulsions and the dispersed water droplets yielded micrometer-size voids in the final aerogel structures. In this context, the results presented in this article on the effects of block copolymer surfactants may be useful in further development of emulsion-templating method for polyimide gels.

EXPERIMENTAL SECTION

Materials. Pyromellitic dianhydride (PMDA) was purchased from Alfa-Aesar (Haverhill, MA), and 2,2′-dimethylbenzidine (DMBZ) was purchased from Shanghai Worldyang Chemical Co. Ltd (Shanghai, China). Tris(2-aminoethyl)amine (TREN) cross-linker and block copolymer surfactant F127 (trademark of BASF) were purchased from Sigma-Aldrich (Milwaukee, WI). Pyridine, acetic anhydride, and acetone were purchased from Fisher Scientific (Ontario, NY). Among the solvents, *N*,*N*-dimethylformamide (DMF) was purchased from VWR International (Radnor, PA), and anhydrous 1-methyl-2-pyrrolidone (NMP) and *N*,*N*-dimethylacetamide (DMAc) were purchased from Sigma-Aldrich (Milwaukee, WI).

DOI: 10.1021/acs.langmuir.8b01513
Langmuir 2018, 34, 8581−8590

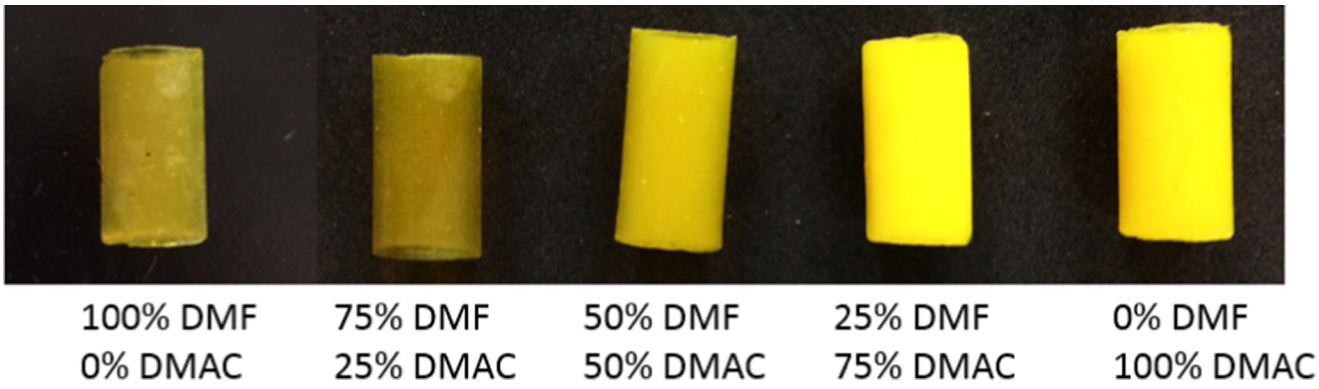

Figure 2. Polyimide aerogels with varying DMF/DMAc solvent compositions (vol %). DMAc vol % increases from left to right.

Fabrication of Polyimide Aerogels. Polyimide gels were synthesized in either a single solvent or a set of mixed solvents. PMDA and DMBZ were dissolved separately in the selected solvent, and the solutions were mixed and magnetically stirred for 2 min at 1200 rpm to form the polyamic acid. Subsequently, TREN, acetic anhydride, and pyridine were added, and the solution was magnetically stirred for 3 min. The solution was subsequently poured into cylindrical molds of a length-to-diameter ratio of 2:1 and allowed to gel. The gels were aged in the molds for 24 h and solvent-exchanged with acetone at least six times to remove the solvent used in synthesis. A typical polyimide gel sample with 7.5 wt % polymer concentration can be prepared using 0.228 g of PMDA, 0.212 g of DMBZ, 0.030 g of TREN, 0.665 g of acetic anhydride, 0.625 g of pyridine, and 5.0 mL of total solvent. A higher than stochiometric amount of TREN cross-linker was used in an effort to obtain aerogels with stronger mechanical properties. The reaction scheme is presented in Figure 1.

The gels were solvent-exchanged with liquid carbon dioxide and dried under supercritical condition of carbon dioxide at 50 °C and 11 MPa pressure. In this work, mixed solvents DMF/NMP and DMF/DMAc were used with the volume percent of DMF at 0, 25, 75, and 100%.

Characterization of Aerogel Materials. *NMR.* Solid-state ^{13}C NMR cross-polarization NMR spectra were collected on a Varian NMRS 500 MHz (11.7 T) spectrometer operated at 125.62 MHz for ^{13}C and equipped with a Varian narrow-bore triple-resonance T3 MAS NMR probe. Samples were packed into 4 mm zirconia rotors and spun about the magic angle at 15 kHz. Cross-polarization experiments were collected with a 40 kHz spectral window, a 0.02 s acquisition time, a 5 s relaxation delay, 16 832 scans, 62.5 kHz cross-polarization and TPPM decoupling fields, and a 1 ms cross-polarization period using a linear-ramped cross-polarization method. The methyl peak of hexamethylbenzene at 17.3 ppm was used as a secondary chemical shift reference.

IR. Infrared spectra were recorded on a Nicolet iS50 FTIR tridetector spectrophotometer (Thermo Scientific, MA).

Elemental Analysis. Elemental analysis was conducted using a 2400 CHNS/O Series II system (Perkin Elmer, MA).

Thermogravimetric Analysis (TGA). Thermogravimetric analysis was conducted under N_2 with a Q50 thermogravimetric analyzer (TA Instruments, DE) using a heating rate of 20 °C/min, up to 700 °C.

Porosity and Pore Volume. Porosity was calculated from the values of skeletal (ρ_s) and bulk density (ρ_b), as shown in eq 1. The values of skeletal density were obtained using a helium pycnometer (AccuPyc II 1340, Micromeritics Instrument Corp., GA). Bulk density was obtained from the mass and volume of the aerogels.

$$\text{porosity} = \left(1 - \frac{\rho_b}{\rho_s}\right) \times 100\% \tag{1}$$

Total pore volume (V_{tot}) was calculated from the bulk and skeletal densities, according to eq 2

$$V_{tot} = \frac{1}{\rho_b} - \frac{1}{\rho_s} \tag{2}$$

Shrinkage. Polyimide gels were synthesized and poured into cylindrical molds of 13 mm diameter. The diameter of the final dried aerogel was measured, and the diameter shrinkage in reference to the original diameter was calculated.

Aerogel Morphology. The morphology of aerogels was studied using a scanning electron microscope (SEM, JSM5310, JEOL, MA). An accelerating voltage of 5 kV and emission current of 20 mA was used to capture the SEM images. A representative piece of fractured aerogel specimen was mounted on an aluminum stub using carbon tape, followed by sputter coating with silver (ISI-5400 Sputter Coater, Polaron, U.K.). Polyimide strand diameter was estimated from SEM images using ImageJ software by considering more than 100 diameter readings for each sample.

Brunauer–Emmett–Teller (BET) Surface Area. Brunauer–Emmett–Teller (BET) surface area of aerogel specimens was obtained from N_2 adsorption–desorption isotherms at 77 K using a Micromeritics Tristar II 3020 analyzer (Micromeritics Instrument Corp. GA). The pore volume of macropores ($V_{macropores}$) was deduced from the total pore volume V_{tot} and the volumes of mesopores ($V_{mesopores}$) and micropores ($V_{micropores}$). For this purpose, CO_2 adsorption–desorption isotherms at 273 K were obtained and combined with the N_2 isotherms using the nonlocal density functional theory model. The fractions of macropores, mesopores, and micropores were then subsequently calculated according to eq 3

$$\varphi_{macropores} = \frac{V_{macropores}}{V_{tot}};\ \varphi_{mesopores} = \frac{V_{mesopores}}{V_{tot}};\ \varphi_{micropores} = \frac{V_{micropores}}{V_{tot}} \tag{3}$$

Compressive Modulus. The compressive modulus of aerogel specimens was obtained from compressive tests using an Instron 5567 tensometer (Norwood, MA) with cylindrical aerogel specimens of a length-to-diameter ratio of 2:1, according to ASTM D695-15.[32] The cylindrical samples were first ground to ensure a smooth, even, and parallel surface and then loaded onto the tensometer. A 1 kN load cell was used, with an extension rate of 1.3 mm/min. The tests were stopped when the force applied exceeded the upper limit of the load cell used. The compressive modulus of the aerogels was obtained from the slope of the stress–strain curve at a low strain, typically 0.01–0.05 mm/mm.

Maximum Bubble Pressure. The mechanical integrity of the polyimide gel was evaluated using a bubble pressure rheometer setup.[33,34] A 22-gauge blunt tip needle attached to a Braintree Scientific syringe pump (Braintree, MA) was used to introduce air at a prescribed pressure. An Omega PX26 pressure transducer connected to an Omega DP25B-S-A process meter and a computer were used to capture pressure readings with time. The gels used in this test were aged for 24 h at room temperature (20 °C). The needle was inserted

DOI: 10.1021/acs.langmuir.8b01513
Langmuir 2018, 34, 8581–8590

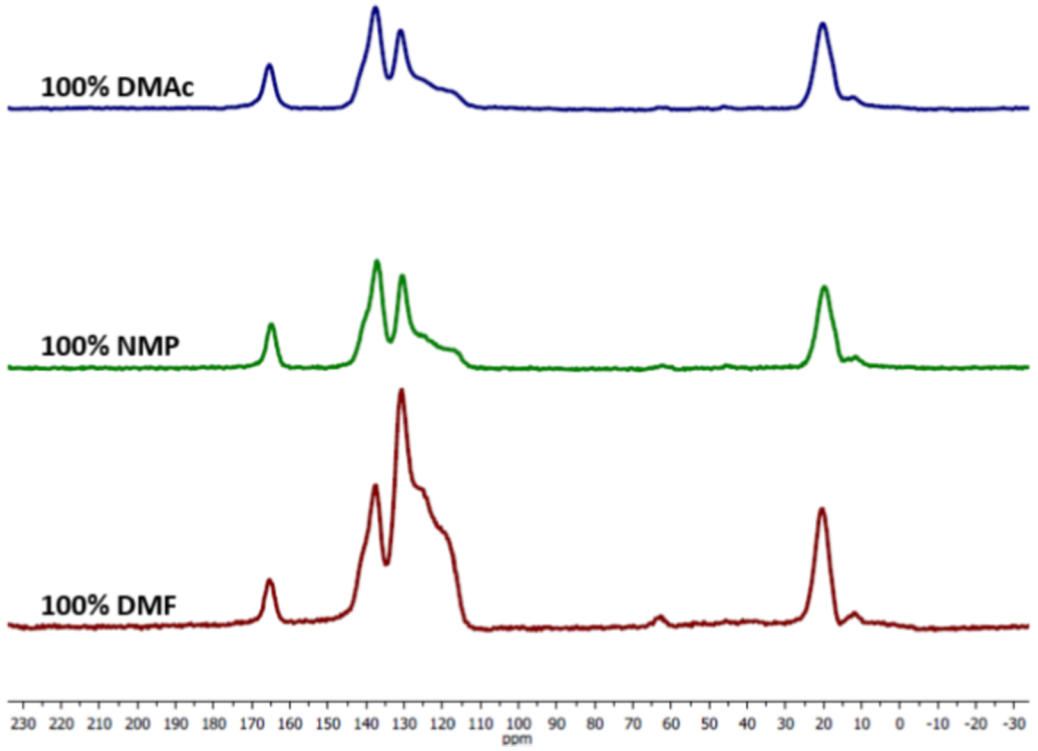

Figure 3. Solid-state ^{13}C NMR spectrum of polyimide synthesized with the 100% DMAc, 100% NMP, and 100% DMF.

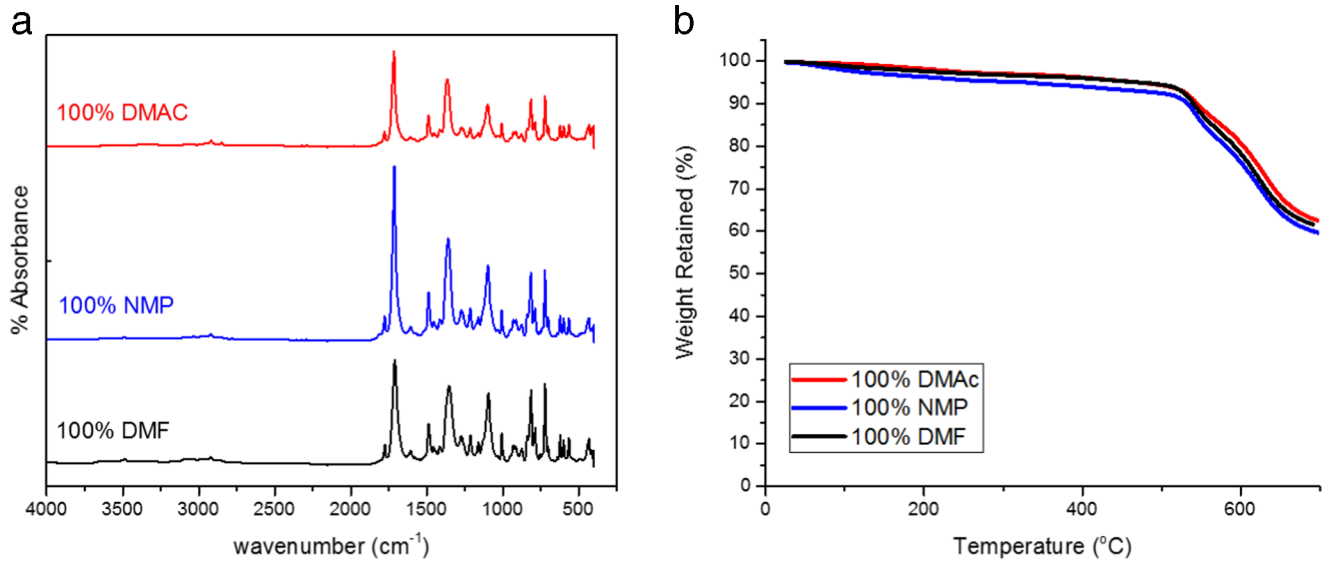

Figure 4. (a) IR spectrum and (b) TGA curves of polyimide synthesized with the 100% DMAc, 100% NMP, and 100% DMF.

approximately at 1 cm below the surface of the gel. Air was pumped into the gel at a flow rate of 5 mL/min, and the pressure reading was recorded for 2 min. The maximum pressure was taken as the critical pressure (P_c) of the gel. Because of high modulus of the polyimide gels, the gels did not experience cavitation at P_c and instead a slight fracture of the gel surrounding the needle occurred, allowing the air to escape and preventing additional increase of pressure in the system.

RESULTS AND DISCUSSION

The aerogels produced in this work appeared amber yellow in color, typical of polyimides (Figure 2). The specimens prepared in neat DMF were translucent, whereas those prepared in NMP and DMAc appeared opaque. Figure 2 shows that the opacity of the aerogels increased with an increase of DMAc fraction in mixed solvent systems DMF/DMAc. A similar transition was observed in DMF/NMP solvent system as well.

The solid-state ^{13}C NMR spectra of polyimide prepared in DMF, NMP, and DMAc are presented in Figure 3. The peaks due to methyl groups (20 ppm) and aromatic carbons (120, 130, and 137 ppm) indicate the inclusion of DMBZ, whereas the peaks of aromatic carbons (130 and 137 ppm) and imide carbonyls (165 ppm) are due to incorporation of PMDA in the polymer structure. In addition, the methylene peaks (62 ppm) confirm that the TREN trifunctional cross-linker was indeed incorporated in the polyimide aerogel structure.

DOI: 10.1021/acs.langmuir.8b01513
Langmuir 2018, 34, 8581−8590

Figure 4a shows the IR spectra of polyimide synthesized with 100% DMAc, NMP, and DMF. All three spectra show the presence of peaks at 730, 1380, 1716, and 1778 cm^{-1}, indicating the presence of the imide functional group. The small peaks at 1620 and 3000 cm^{-1} indicate the presence of small amounts of polyamic acid that did not undergo imidization. The absence of peaks at 3250−3400 cm^{-1} also confirm the absence of primary amine groups in imidized materials. The TGA traces of aerogels synthesized with single solvents are shown in Figure 4b. It is apparent that the three materials have similar TGA traces, exhibiting weight loss of 6−9 wt % until about 525 °C, after which the degradation of polyimide began. We attribute the small weight loss observed up to 525 °C to thermal degradation of the residual polyamic acid, as earlier discussed in the context of IR spectra in Figure 4a. The small weight loss observed before 525 °C is consistent with the TGA data of other polyimide aerogel materials reported in the literature.[35] At 700 °C, all three TGA traces show char yield of ∼60 wt %.

The absence of free amine groups in imidized materials is corroborated by the data from elemental analysis, as listed in Table 1. The molar ratio of nitrogen/carbon (N/C) for all three aerogel specimens fell in the range 0.083−0.085, close to the theoretical molar N/C ratio 0.083 in one PMDA/DMBZ repeat unit. This suggests that the polyimide polymer was comprised primarily of PMDA and DMBZ monomers with small contribution from TREN. Note that TREN cross-linker has a molar N/C ratio of 0.66. The close molar N/C ratio of the final aerogel material to that of the polymeric repeat unit was earlier observed by Leventis et al.[36] The slightly higher N/C ratio observed for aerogels synthesized with 100% DMAc indicates a shorter oligomer chain length and slightly higher ratio of TREN cross-linker.

Table 1. Elemental Analysis of Polyimide Synthesized with 100% DMAc, 100% NMP, and 100% DMF

	elemental analysis (wt %)			
solvent	C	H	N	molar N/C
100% DMF	71.15	3.37	6.87	0.083
100% NMP	70.29	3.57	6.84	0.084
100% DMAc	70.33	3.41	6.97	0.085

The data on diameter shrinkage, bulk and skeletal density, porosity, and gel times of specimens prepared in various solvent systems are listed in Table 2. In the case of mixed solvents, various volume fractions of DMF with NMP and DMF with DMAc were used. Polyimide aerogels prepared in DMF exhibited a diameter shrinkage of 13.6%, whereas those prepared in NMP and DMAc had diameter shrinkage of 9−10%. Such moderate shrinkage values can be attributed to capillary stress originating from the evaporation of residual synthesis solvents in the heating phase of the supercritical drying step.

The data in Table 2 also reflect that the skeletal density of the aerogel specimens remained relatively constant in the range 1.36−1.39 g/cm^3, whereas the bulk density varied from 0.07 g/cm^3 for specimens prepared in 100% DMF to 0.06 g/cm^3 for 100% NMP to 0.056 g/cm^3 for 100% DMAc. The bulk density values for specimens prepared in solvent mixtures fell within the range of corresponding single-solvent data. The porosity of aerogel specimens fell within a narrow range of 94.9−96.0%.

One key observation from the data listed in Table 2 is the effect of single solvent on gel time; e.g., polyimide synthesized in 100% DMF turned into a gel in about 6.5 min, whereas the system with the same polymer content gelled in 112 min in NMP and in 109 min in DMAc. The gel times in the case of mixed solvents fell within the window of corresponding single solvents. At gel time, the liquid meniscus in the mold did not show movement when the mold was tilted at an angle.

Two factors are responsible for dependence of gel times on solvents. First, higher solubility of polyimide in a solvent can delay its phase separation into solid polymer nodules that subsequently interconnect and form the strands in the gel networks, as was recently established for polybenzoxazine system.[37] However, such differences in solubility alone cannot explain the huge differences in gel times reported in Table 2. In view of this, we invoke a second factor, which is the increased reaction rates brought about by the electron accepting properties of the solvents. Adopting Gutmann's scale of acceptor numbers (AN), Table 3 shows that the electron

Table 3. Surface Tension, Donor Number (DN), Acceptor Number (AN), and $E_T(30)$ of Solvents[a]

		electron donating	electron accepting	
solvent	surface tension@17 °C (mN/m)	donor number (kcal/mol)	acceptor number	$E_T(30)$ (kcal/mol)
DMF	37.0 ± 0.0	26.6	16	43.2
NMP	41.0 ± 0.1	27.3	13.3	42.2
DMAc	36.0 ± 0.0	27.8	13.6	42.9

[a]Surface tension was measured, whereas DN, AN, and $E_T(30)$ were obtained from Reichardt.[19]

Table 2. Shrinkage, Bulk Density, Skeletal Density, Porosity, and Gel Times of Polyimides Synthesized with Various Solvent Compositions

solvent composition (vol %)							
DMF	NMP	DMAC	shrinkage (%)	bulk density (g/cm^3)	skeletal density (g/cm^3)	porosity (%)	gel time (min)
100			13.6 ± 0.0	0.070 ± 0.001	1.36 ± 0.04	94.9 ± 0.1	6.5
75	25		12.6 ± 0.3	0.066 ± 0.001	1.39 ± 0.04	95.2 ± 0.0	23
50	50		11.2 ± 0.0	0.063 ± 0.000	1.36 ± 0.04	95.4 ± 0.0	44
25	75		9.0 ± 0.0	0.056 ± 0.001	1.39 ± 0.04	96.0 ± 0.0	89
	100		9.7 ± 0.3	0.060 ± 0.000	1.37 ± 0.04	95.6 ± 0.0	112
75		25	12.7 ± 0.0	0.066 ± 0.000	1.36 ± 0.05	95.1 ± 0.1	23
50		50	8.7 ± 0.3	0.056 ± 0.003	1.37 ±0.04	95.9 ± 0.1	56
25		75	9.0 ± 0.2	0.056 ± 0.001	1.36 ± 0.03	95.9 ± 0.1	70
		100	9.2 ± 0.0	0.056 ± 0.001	1.36 ± 0.03	95.9 ± 0.1	109

DOI: 10.1021/acs.langmuir.8b01513
Langmuir 2018, 34, 8581−8590

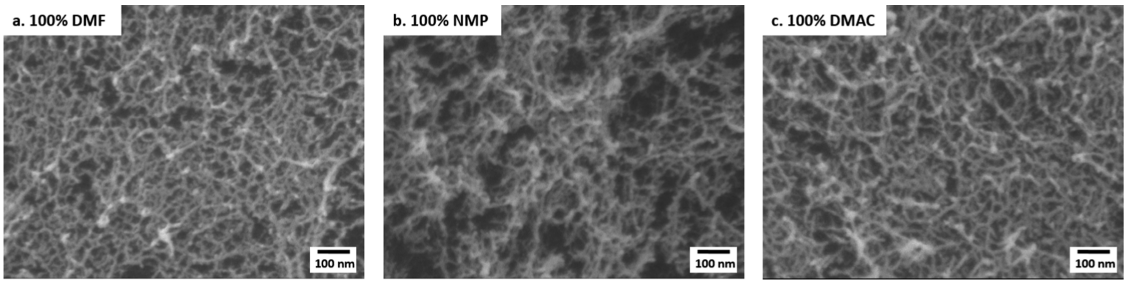

Figure 5. SEM images of polyimides prepared using (a) DMF, (b) NMP, and (c) DMAc.

Table 4. BET Surface Area, Pore Volume, and Micro, Meso, and Macropore Fraction of Polyimides Synthesized with Various Solvent Compositions

solvent composition (vol %)							
DMF	NMP	DMAC	BET surface area (m^2/g)	pore volume (cm^3/g)	micropore fraction (<2 nm)	mesopore fraction (2−50 nm)	macropore fraction (>50 nm)
100			792 ± 5	13.5 ± 0.1	0.015	0.511	0.474
75	25		760 ± 21	14.3 ± 0.1	0.010	0.155	0.835
50	50		573 ± 10	15.2 ± 0.1	0.009	0.124	0.867
25	75		485 ± 11	17.1 ± 0.1	0.010	0.081	0.909
	100		457 ± 16	15.9 ± 0.2	0.010	0.045	0.945
75		25	752 ± 24	14.3 ± 0.1	0.008	0.163	0.829
50		50	552 ± 21	17.2 ± 1.2	0.007	0.041	0.952
25		75	474 ± 10	17.1 ± 0.4	0.005	0.039	0.956
		100	443 ± 11	17.0 ± 0.2	0.007	0.031	0.962

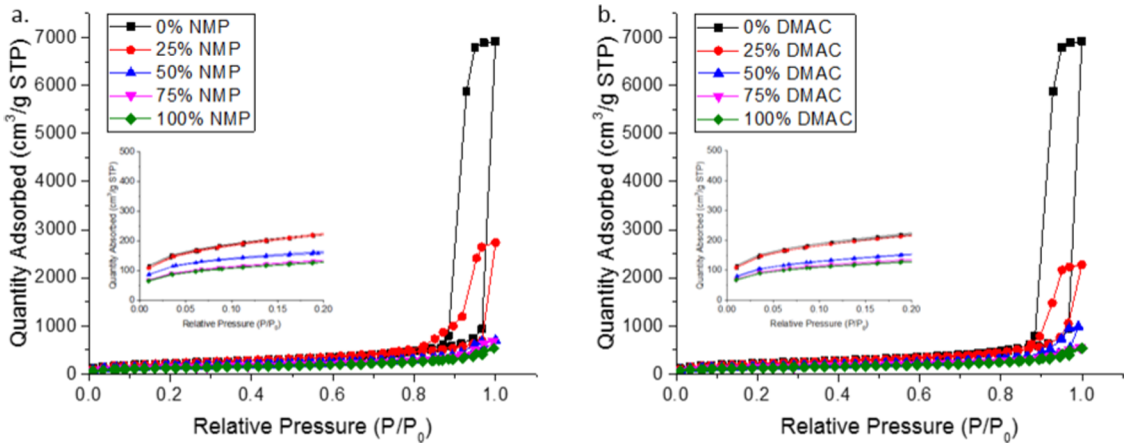

Figure 6. BET isotherms of polyimide aerogels with increasing (a) NMP and (b) DMAc content in the synthesis solvent.

accepting properties of the solvents increase in the order of NMP < DMAc < DMF. This means that DMF with higher electron accepting capability should exhibit higher Lewis acid behavior. A more acidic solvent stabilizes the activated complex of the polyamic acid and drives the reaction forward. This is supported by other studies on polyamic acid kinetics.[38,39] Kaas[38] showed that the polyamic acid reaction exhibits a sigmoidal-shaped concentration versus time curve indicative of a second order, equilibrium controlled, autocatalytic reaction. It was also reported that polyamic acid formation reaction is acid catalyzed, instead of base catalyzed.[38,40] In a separate study, Solomin et al.[39] reported higher rates of polyamic acid formation in acidic solvents such as *m*-cresol and acetonitrile than in more basic solvents such as tetrahydrofuran.

An increase in gel times compared with DMF due to use of NMP, DMAc, or their mixtures with NMP also produced changes in the morphology of the corresponding aerogels. These changes will be gleaned from the SEM images (Figure 5) and from the BET data listed in Table 4.

Figure 5 shows that the aerogel specimens contained similar fibrillar structures, with the polyimide strand size increasing with an increase of gel time. Polyimides prepared with 100% DMF gelled in 6.5 min and had a corresponding strand size of 9.3 ± 1.7 nm, whereas those prepared with NMP and DMAc had strand sizes of 13.5 ± 3.1 and 14.8 ± 2.5 nm, respectively, corresponding to higher gel times of 112 and 109 min. The data in Tables 2 and 4 show that BET surface area reduced with an increase of gel time. In the mixed solvent system of DMF with NMP, the gel time increased with NMP content from 6.5 min for 100% DMF to 112 min for 100% NMP. The

DOI: 10.1021/acs.langmuir.8b01513
Langmuir 2018, 34, 8581−8590

corresponding aerogel specimens showed BET surface area reduction from 792 m^2/g for 100% DMF to 457 m^2/g for 100% NMP. The same trend is prevalent in systems containing DMAc; the BET surface area with 100% DMAc is 443 m^2/g.

In light of negligible changes in skeletal density of the aerogel specimens in different solvents (Table 2), one can attribute the reduction in specific surface area to coarsening of polymer strands. For polyimide strands of cylindrical shape, as seen in Figure 5, the specific surface area scales inversely with the strand diameter. Recall that mean polymer strand diameter and specific surface area of polyimide aerogels synthesized in DMF were, respectively, 9.3 nm and 792 m^2/g. In reference to these values, polyimide aerogels synthesized in NMP (mean strand diameter 13.5 nm) and DMAc (mean strand diameter 14.8 nm) should have specific surface areas of 546 and 497 m^2/g, respectively. The experimental data in Table 4 indicate surface areas of 457 and 443 m^2/g, respectively, for the two systems, in each case showing reduction.

The coarsening of polymer strands should have an impact on the volume fractions of different types of pores. Of these, micropore fraction is anticipated to be much less affected; polyimide strands do not contain inherent micropores unlike syndiotactic polystyrene systems.[8] Thus, all micropores in polyimide aerogels are formed due to crossover of the adjoining strands. The data in Table 4 show the following trends with an increase of NMP content from 0 to 100% in the solvent system: (i) as anticipated, the micropore fraction reduced only slightly from 0.015 to 0.010, (ii) the mesopore fraction reduced significantly from 0.511 to 0.045, and (iii) the macropore fraction increased from 0.474 to 0.945. A reduction of mesopore content with an increase of NMP and DMAc fractions is gleaned from a smaller area under the hysteresis loops in the BET isotherms, as presented in Figure 6. The specimens obtained with DMF show the largest area under the hysteresis loop, whereas those obtained with NMP or DMAc show a negligible area. This shift from almost a 50:50 ratio of meso- and macropores obtained using DMF to predominantly macropores in the case of NMP and DMAc also correlates well with the shrinkage data reported in Table 2. Aerogel specimens with larger mesopore fractions underwent higher shrinkage due to greater capillary stress originating from smaller pores. In this context, the shift to pore sizes from a primarily mesoporous state to majority macroporous state can also account for the increase of opacity of the aerogels, as shown in Figure 2. The larger pores approaching the wavelength of light enable scattering of incident light and contribute to opacity. Corresponding pore size distributions of the aerogel specimens are presented in Figure S1.

We now focus attention on why the strand size increased in systems that showed longer gel times. In polyimide system, gelation occurs via a sequence of steps. First, the oligomer molecular weight increases with conversion. The system then undergoes polymerization-induced phase separation, as the binodal line in a temperature-composition diagram gradually shifts upward toward the experimental temperature with an increase of molecular weight. Once in the binodal region, the system phase separates into a polymer-rich region, which turns into the strands in aerogel and a solvent-rich region, which later turns into the pores in aerogel. These phase-separated regions coarsen over time, before the system reaches the sol–gel transition and vitrifies due to high conversions and cross-linking densities.[41] At lower rates of polymerization, i.e., at longer gel times, the sol–gel transition after phase separation is prolonged. This promotes coarsening of the polymer-rich domains in an attempt to reduce the unfavorable interfacial area with the liquid-rich domains and leads to thicker polymer strands in the gel.

The values of compressive modulus of polyimide aerogels synthesized in various solvents are listed in Table 5. The aerogels synthesized in DMF show the highest value of the compressive modulus at 44.6 MPa, whereas those synthesized in NMP and DMAc show compressive modulus of 8.9 and 5.8 MPa, respectively. The aerogels synthesized in mixed solvents show modulus values within the bounds of materials produced in single solvents.

Table 5. Compressive Modulus of Polyimide Aerogels Synthesized with Various Solvent Compositions

solvent composition (vol %)			
DMF	NMP	DMAc	compressive modulus (MPa)
100			44.6 ± 1.3
75	25		23.4 ± 2.0
50	50		16.2 ± 2.9
25	75		7.9 ± 0.4
	100		8.9 ± 1.7
75		25	28.7 ± 1.8
50		50	13.5 ± 1.6
25		75	10.6 ± 2.2
		100	5.8 ± 4.4

The aerogel specimens synthesized in DMAc exhibited brittle fracture, whereas those synthesized in DMF and NMP show yielding behavior, as gleaned from the representative stress vs strain curves in Figure 7. This brittle failure can be attributed to the reduced number of cross-links in the system due to the shift in the equilibrium to the left of the polyamic acid reaction in a more basic solvent, thus reducing the overall conversion. The stress vs strain curves of materials synthesized in DMF and NMP are typical of porous materials, comprising of three main regions. As per Swyngedau,[42] the first region involves the deformation of the aerogel matrix at a strain of 0–0.04 mm/mm with the applied load borne by the skeletal structure of the cross-linked polymer networks. In the second

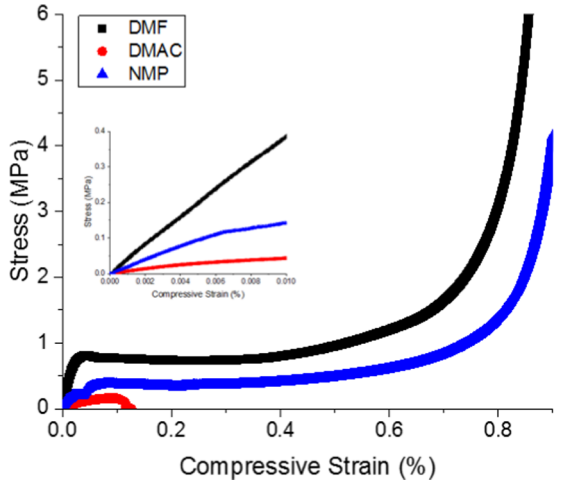

Figure 7. Representative compressive stress/strain curves of polyimide aerogels synthesized with 100% DMF, 100% NMP, and 100% DMAc.

DOI: 10.1021/acs.langmuir.8b01513
Langmuir 2018, 34, 8581–8590

Table 6. Strand Diameter, BET Surface Area, Micropore, Mesopore, and Macropore Fraction of Polyimide Aerogels with F127 Surfactant

surfactant concentration (vol %)	strand diameter (nm)	BET surface area (m^2/g)	micropore fraction (<2 nm)	mesopore fraction (2−50 nm)	macropore fraction (>50 nm)	gel time (min)
0	9.3 ± 1.7	792 ± 5	0.015	0.511	0.474	6.5
0.5	15.5 ± 3.8	544 ± 27	0.014	0.077	0.909	14
2.5	19.9 ± 3.4	426 ± 30	0.010	0.057	0.933	17
5	30.4 ± 6.3	286 ± 17	0.006	0.041	0.953	29

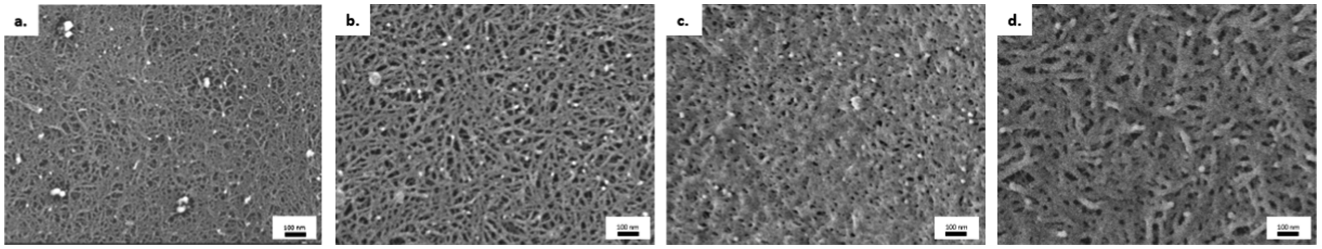

Figure 8. SEM images of polyimide aerogels with F127 surfactant concentration of (a) 0 vol %, (b) 0.5 vol %, (c) 2.5 vol %, and (d) 5.0 vol %. Images were taken of the surface of the aerogel monolith to facilitate measurement of strand size.

region, at a strain from 0.04 to 0.7 mm/mm, the skeletal structure collapses, leading to densification of the pores. All pores are compacted, and the load is borne by the now compressed bulk polymer in the third region at a strain >0.7 mm/mm. The aerogels synthesized in DMAc exhibited brittle failure at a strain of around 0.1 mm/mm.

Control of Pore Size Distribution Through Addition of Surfactant. The data discussed up to this point established that at longer gel times, the chosen solvent systems produced thicker polyimide strands, higher fractions of macropores, and inferior compressive modulus values. Therefore, it is not meaningful to control the gel times through manipulation of solvent composition if one is interested in achieving significant macropores and strong compressive properties. An alternative is to stick to an aprotic solvent with high AN, such as DMF for synthesis of aerogels, but manipulate the gel times via alteration of the viscosity of the solution and solubility by some other means. In this context, a poly(ethylene oxide) (PEO)−poly(propylene oxide)−PEO block copolymer (F217) was added as viscosity modifier of the solution. Specifically, the block copolymer was included in the initial synthesis step by first dissolving it in DMF. The viscosity vs surfactant concentration data presented in Figure S2 show an increase of viscosity by more than 2-fold at 5 vol % of the surfactant. The idea is that an increase in viscosity of the solution would shift the reactions to the diffusion-controlled regime and allow longer times for phase separation and coarsening of polymer strands. In conjunction, a high AN solvent helps maintain the equilibrium and high conversion, thus generating aerogels with desired mechanical strength.

The presence of surfactant indeed increased the gel time, as shown in Table 6, with the highest surfactant concentration of 5 vol % increasing the gel time from 6.5 min for DMF with no surfactant to 29 min. The polymer strand size also increased with an increase of surfactant concentration. This can be seen from SEM images in Figure 8 and the values of strand diameters measured from SEM images and listed in Table 6. The strand diameters increased from 9.3 nm for the system with no surfactant to 15.5 nm for that with 0.5 vol % surfactant to 19.9 nm for that with 2.5 vol % surfactant to 30.4 nm for that with 5 vol % surfactant concentration. The scatter of the data increased at higher surfactant concentration. The increase of polymer strand diameter with surfactant concentration also led to reduction of BET surface area, e.g., 792 m^2/g for the case with no surfactant to 286 m^2/g for the system with 5 vol % surfactant, as listed in Table 6. The inclusion of surfactants also led to shifting of micro, meso, and macropore fractions (Table 6). The most significant changes occurred in the fractions of meso- and macropores. For example, the presence of 0.5 vol % surfactant caused a reduction of mesopore fraction from 0.511 to 0.077 and increase of macropore fraction from 0.474 to 0.909. Additional surfactants at 5 vol % produced aerogel systems with meso- and macropore fractions at 0.041 and 0.953, respectively. The reduction in BET surface area and mesopore fractions are evident from the BET isotherms presented in Figure 9.

Next, the compressive modulus values of gels and corresponding aerogels were determined. The compressive modulus of gels was obtained from pressure versus time curves shown in Figure 10 for a set of representative polyimide gels.

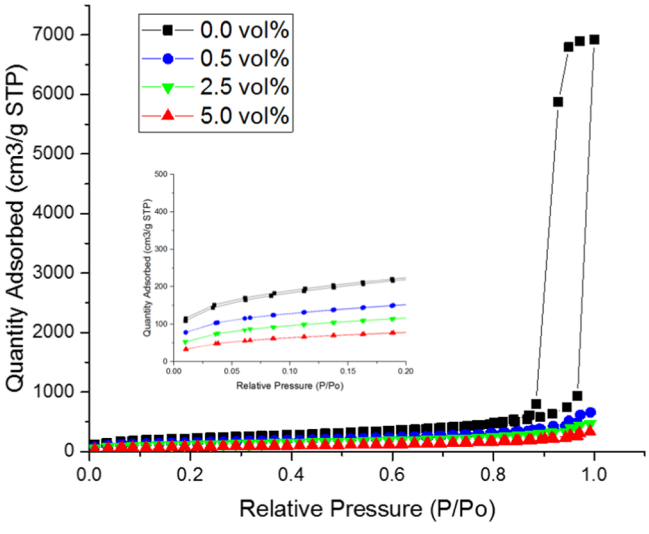

Figure 9. BET isotherms of polyimide aerogels with various F127 surfactant concentrations.

DOI: 10.1021/acs.langmuir.8b01513
Langmuir 2018, 34, 8581−8590

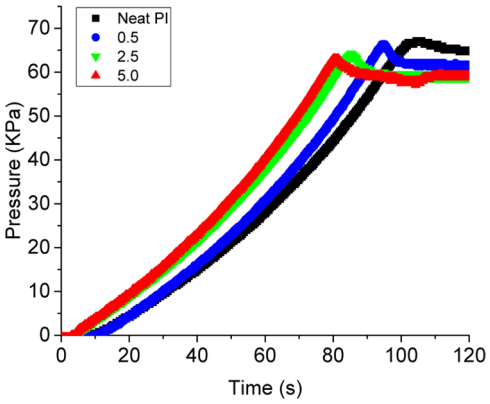

Figure 10. Bubble pressure vs time pressure curves of neat polyimide gel and polyimide gel with surfactant.

The maximum values of pressure (critical pressure) are listed in Table 7. As is intuitive, pressure first increased with time, reaching a maximum pressure, called the critical pressure, then dropped slightly, and finally reached a plateau. At critical pressure, the gel structure undergoes yield and fractures in selective locations, thus allowing high-pressure air to escape via the gel−solid interface of the container. The critical pressure can be used as an analogue of mechanical strength of the gel. From the data presented in Figure 10 and Table 7, one can infer that the mechanical strength of the gel was weakly dependent on surfactant concentration. The same trend is evident for the data on compressive modulus of aerogels in Table 7, also measured using an Instron 5567 tensometer.

Table 7. Maximum Pressure and Compressive Modulus of Neat Polyimide and Polyimide with Surfactant

surfactant concentration (vol %)	critical pressure (kPa)	compressive modulus (MPa)
0.0	66.8 ± 0.4	44.5 ± 1.3
0.5	66.4 ± 0.0	44.1 ± 2.6
2.5	64.5 ± 0.8	44.1 ± 1.1
5	63.2 ± 0.2	38.3 ± 2.7

The above sets of data established that the inclusion of F127 surfactant led to a slow-down of gelation, coarsening of polymer strand diameter, and reduction of mesopore fraction, but did not cause reduction of compressive modulus values, unlike in the cases where NMP and DMAc were used as the solvents. Table 5 shows that the compressive modulus of aerogels synthesized with 100% NMP and 100% DMAc were 8.9 and 5.8 MPa, respectively, whereas an aerogel with 5 vol % surfactant in 100% DMF exhibited a compressive modulus of 38.3 MPa. These aerogel specimens had similar macropore fractions of around 0.95.

CONCLUSIONS

The results presented in this article show that several properties of polyimide aerogels, such as polymer strand diameter, mesopore and macropore fractions, specific surface area, and compressive modulus can be manipulated via a selection of appropriate solvents and concentration of a block copolymer surfactant during preparation of corresponding polymer gels. The time of gelation can be prolonged via a selection of electron donating solvents, such as DMAc and NMP, or inclusion of a block copolymer surfactant that increases the viscosity of the medium. In these cases, a slow-down of gelation also led to coarsening of polymer strands, which in turn adversely affected BET surface area and mesopore fractions. However, the compressive modulus of polyimide aerogels reduced significantly when NMP and DMAc were used in synthesis. On the other hand, the inclusion of surfactants did not compromise the compressive modulus of aerogels or the mechanical strength of polyimide gels.

ASSOCIATED CONTENT

Supporting Information

The Supporting Information is available free of charge on the ACS Publications website at DOI: 10.1021/acs.langmuir.8b01513.

Pore size distribution of aerogels with increasing (a) NMP and (b) DMAc content; effect of surfactant concentration on viscosity of DMF solution (PDF)

AUTHOR INFORMATION

Corresponding Author

*E-mail: janas@uakron.edu.

ORCID

Sadhan C. Jana: 0000-0001-8962-380X

Notes

The authors declare no competing financial interest.

ACKNOWLEDGMENTS

Authors acknowledge K. Cavicchi of University of Akron for allowing the use of bubble pressure rheometer setup.

REFERENCES

(1) Kistler, S. Coherent Expanded Aerogel Jellies. *Nature* **1931**, *127*, 741.

(2) Yoldas, B. E.; Annen, M. J.; Bostaph, J. Chemical Engineering of Aerogel Morphology Formed under Nonsupercritical Conditions for Thermal Insulation. *Chem. Mater.* **2000**, *12*, 2475−2484.

(3) Zhai, C.; Jana, S. C. Tuning Porous Networks in Polyimide Aerogels for Airborne Nanoparticle Filtration. *ACS Appl. Mater. Interfaces* **2017**, *9*, 30074−30082.

(4) Kim, S. J.; Chase, G.; Jana, S. C. Polymer Aerogels for Efficient Removal of Airborne Nanoparticles. *Sep. Purif. Technol.* **2015**, *156*, 803−808.

(5) Kim, S. J.; Jana, S. C. Effects of Skin Layers on Air Permeability in Macroporous Polymer Aerogels. *Polymer* **2017**, *126*, 432−436.

(6) Kim, S. J.; Raut, P.; Jana, S. C.; Chase, G. Electrostatically Active Polymer Hybrid Aerogels for Airborne Nanoparticle Filtration. *ACS Appl. Mater. Interfaces* **2017**, *9*, 6401−6410.

(7) Kim, S. J.; Chase, G.; Jana, S. C. The Role of Mesopores in Achieving High Efficiency Airborne Nanoparticle Filtration Using Aerogel Monoliths. *Sep. Purif. Technol.* **2016**, *166*, 48−54.

(8) Daniel, C.; Dammer, C.; Guenet, J.-M. On the Definition of Thermoreversible Gels: The Case of Syndiotactic Polystyrene. *Polymer* **1994**, *35*, 4243−4246.

(9) Brinker, C. J.; Scherer, G. *Sol-Gel Science: The Physics and Chemistry of Sol-Gel Processing*; Academic Press, 2013.

(10) Shinko, A.; Jana, S. C.; Ann Meador, M. Crosslinked Polyurea Aerogels with Controlled Porosity. *RSC Adv.* **2015**, *5*, No. 105329.

(11) Guo, H.; Meador, M. A. B.; McCorkle, L.; Quade, D. J.; Guo, J.; Hamilton, B.; Cakmak, M.; Sprowl, G. Polyimide Aerogels Cross-Linked through Amine Functionalized Polyoligomeric Silsesquioxane. *ACS Appl. Mater. Interfaces* **2011**, *3*, 546−552.

(12) Meador, M. A. B.; Malow, E. J.; He, Z. J.; McCorkle, L.; Guo, H.; Nauyen, B. Synthesis and Properties of Nanoporous Polyimide

DOI: 10.1021/acs.langmuir.8b01513
Langmuir 2018, 34, 8581−8590

Aerogels Having a Covalently Bonded Network Structure. *Polym. Prepr.* **2010**, *51*, 265.
(13) Gu, S.; Li, Z.; Miyoshi, T.; Jana, S. C. Polybenzoxazine aerogels with controllable pore structures. *RSC Adv.* **2015**, *5*, 26801−26805.
(14) Rao, A. V.; Pajonk, G. M.; Parvathy, N. N. Effect of Solvents and Catalysts on Monolithicity and Physical Properties of Silica Aerogels. *J. Mater. Sci.* **1994**, *29*, 1807−1817.
(15) Leventis, N.; Chidambareswarapattar, C.; Bang, A.; Sotiriou-Leventis, C. Cocoon-in-Web-Like Superhydrophobic Aerogels from Hydrophilic Polyurea and Use in Environmental Remediation. *ACS Appl. Mater. Interfaces* **2014**, *6*, 6872−6882.
(16) Buncel, E.; Stairs, R. A. Dipolar Aprotic Solvents. In *Solvent Effects in Chemistry*; John Wiley & Sons, Inc, 2015; pp 140−154.
(17) Miller, J.; Parker, A. J. Dipolar Aprotic Solvents in Bimolecular Aromatic Nucleophilic Substitution Reactions1. *J. Am. Chem. Soc.* **1961**, *83*, 117−123.
(18) Parker, A. J. Protic-Dipolar Aprotic Solvent Effects on Rates of Bimolecular Reactions. *Chem. Rev.* **1969**, *69*, 1−32.
(19) Reichardt, C. *Solvents and Solvent Effects in Organic Chemistry*; Wiley-VCH Verlag GmbH & Co.: Weinham, Germany, 2003; pp 1−84.
(20) Reichardt, C. Solvents and Solvent Effects: An Introduction. *Org. Process Res. Dev.* **2007**, *11*, 105−113.
(21) Gutmann, V. Empirical Parameters for Donor and Acceptor Properties of Solvents. *Electrochim. Acta* **1976**, *21*, 661−670.
(22) Mayer, U.; Gutmann, V.; Gerger, W. The Acceptor Number — A Quantitative Empirical Parameter for the Electrophilic Properties of Solvents. *Monatsh. Chem.* **1975**, *106*, 1235−1257.
(23) Kosower, E. M. The Effect of Solvent on Spectra. I. A New Empirical Measure of Solvent Polarity: Z-Values. *J. Am. Chem. Soc.* **1958**, *80*, 3253−3260.
(24) Schmid, R. Effect of Solvent on Chemical Reactions and Reactivity. *Handb. Solvents* **2001**, 737−846.
(25) Fawcett, W. R. Acidity and Basicity Scales for Polar Solvents. *J. Phys. Chem.* **1993**, *97*, 9540−9546.
(26) Marcus, Y. The Effectivity of Solvents as Electron Pair Donors. *J. Solution Chem.* **1984**, *13*, 599−624.
(27) Edwards, W. M.; Maxwell, R. I. Polyimides of Pyromellitic Acid. U.S. Patent US2710853A, 1955.
(28) Ghosh, M.; Mittal, K. L. *Polyimides: Fundamentals and Applications*; Marcel Dekker Inc.: New York, 1996; pp 7−21.
(29) Wilson, D.; Stenzenberger, H.; Hergenrother, P. M. *Polyimides*; Chapman and Hall: New York, 1990; pp 1−35.
(30) Alexander, R.; Ko, E.; Parker, A.; Broxton, T. Solvation of Ions. XIV. Protic-Dipolar Aprotic Solvent Effects on Rates of Bimolecular Reactions. Solvent Activity Coefficients of Reactants and Transition States at 25°. *J. Am. Chem. Soc.* **1968**, *90*, 5049−5069.
(31) Teo, N.; Jana, S. C. Open Cell Aerogel Foams via Emulsion Templating. *Langmuir* **2017**, *33*, 12729−12738.
(32) ASTM D695-15, *Standard Test Method for Compressive Properties of Rigid Plastics*; ASTM International: West Conshocken, PA, 2015.
(33) Fei, P.; Wood, S. J.; Chen, Y.; Cavicchi, K. A. Maximum Bubble Pressure Rheology of Low Molecular Mass Organogels. *Langmuir* **2015**, *31*, 492−498.
(34) Zimberlin, J. A.; Crosby, A. J. Water Cavitation of Hydrogels. *J. Polym. Sci., Part B: Polym. Phys.* **2010**, *48*, 1423−1427.
(35) Chidambareswarapattar, C.; Larimore, Z.; Sotiriou-Leventis, C.; Mang, J. T.; Leventis, N. One-step room-temperature synthesis of fibrous polyimide aerogels from anhydrides and isocyanates and conversion to isomorphic carbons. *J. Mater. Chem.* **2010**, *20*, 9666−9678.
(36) Leventis, N.; Sotiriou-Leventis, C.; Mohite, D. P.; Larimore, Z. J.; Mang, J. T.; Churu, G.; Lu, H. Polyimide Aerogels by Ring-Opening Metathesis Polymerization (ROMP). *Chem. Mater.* **2011**, *23*, 2250−2261.
(37) Li, H.; Gu, S.; Thomas, S.; Liu, T.; Jana, S. C. Investigation of Polybenzoxazine Gelation Using Laser Light Scattering. *J. Appl. Polym. Sci.* **2018**, *135*, No. 45709.
(38) Kaas, R. L. Autocatalysis and Equilibrium in Polyimide Synthesis. *J. Polym. Sci., Polym. Chem. Ed.* **1981**, *19*, 2255−2267.
(39) Solomin, V.; Kardash, I.; Snagovskii, I.; Messerle, P.; Zhubanov, B.; Pravednikov, A. Features Of Kinetics Of Amine Acylation By Anhydrides Of Aromatic And Alicyclic Carboxylic-Acids. *Dokl. Akad. Nauk SSSR* **1977**, *236*, 139−142.
(40) Takekoshi, T. Polyimides. In *Kirk-Othmer Encyclopedia of Chemical Technology*; John Wiley & Sons, Inc., 2000.
(41) Nakanishi, K.; Soga, N. Phase Separation in Silica Sol-Gel System Containing Polyacrylic Acid I. Gel Formation Behavior and Effect of Solvent Composition. *J. Non-Cryst. Solids* **1992**, *139*, 1−13.
(42) Swyngedau, S.; Nussinovitch, A.; Peleg, M. Models for the Compressibility of Layered Polymeric Sponges. *Polym. Eng. Sci.* **1991**, *31*, 140−144.

DOI: 10.1021/acs.langmuir.8b01513
Langmuir 2018, 34, 8581−8590